A Facile Approach toward Multicomponent Supramolecular Structures: Selective Self-Assembly via Charge Separation

ARTICLE *in* JOURNAL OF THE AMERICAN CHEMICAL SOCIETY · NOVEMBER 2010

Impact Factor: 12.11 · DOI: 10.1021/ja106251f · Source: PubMed

7 AUTHORS, INCLUDING:

Koushik Ghosh
Los Alamos National Laboratory
30 PUBLICATIONS **1,081** CITATIONS

Published in final edited form as:
J Am Chem Soc. 2010 December 1; 132(47): 16873–16882. doi:10.1021/ja106251f.

A Facile Approach Towards Multicomponent Supramolecular Structures: Selective Self-Assembly via Charge Separation

Yao-Rong Zheng[*], **Zhigang Zhao**, **Ming Wang**, **Koushik Ghosh**, **J. Bryant Pollock**, **Timothy R. Cook**, and **Peter J. Stang**[*]
Department of Chemistry, University of Utah, 315 South 1400 East, RM, 2020, Salt Lake City, Utah, 84112

Abstract

A novel approach towards the construction of multicomponent two-dimensional (2-D) and three-dimensional (3-D) metallosupramolecules is reported. Simply by mixing carboxylate and pyridyl ligands with *cis*-$Pt(PEt_3)_2(OTf)_2$ in a proper ratio, coordination-driven self-assembly occurs, allowing for selective generation of discrete multicomponent structures via charge separation on the metal centers. Using this method, a variety of 2-D rectangles and 3-D prisms were prepared under mild conditions. Moreover, multicomponent self-assembly can also be achieved by supramolecule-to-supramolecule transformations. The products were characterized by ^{31}P and ^{1}H multinuclear NMR spectroscopy, electrospray ionization mass spectrometry (ESI-MS), and pulsed-field-gradient spin echo (PGSE) NMR techniques together with computational simulations.

Keywords

Multicomponent Supramolecular Structures; Selective Self-Assembly; Coordination-Driven Self-Assembly; Supramolecular Rectangle; Supramolecular Prisms; Supramolecular Transformation

Introduction

Over the last decade, coordination-driven self-assembly has evolved into a well-established methodology for constructing novel metallosupramolecular structures using dative metal-ligand bonding interactions. A variety of elaborate metallosupramolecules, from two-dimensional (2-D) polygons to three-dimensional (3-D) cages, prisms, and polyhedra, have been reported based on coordination-driven self-assembly.[1] By virtue of the resulting well-defined structures, coordination-driven self-assembly has a wide range of applications, such as synthesis of metallosupramolecular dendrimers,2 encapsulation of guests,3 and uses in catalysis4 and sensors.[5] However, the design of coordination-driven self-assembly has been mostly constrained to two-component systems, in which only one metallic and one organic component is used.[1] The two-component approach endows coordination-driven self-assembly with easy control and design, but significantly limits the versatility of molecular components involved, and, therefore, the diversity of the resulting supramolecules.[6] In order to broaden the diversity of coordination-driven self-assembly, it is essential to explore controlled self-assembly within a multicomponent system.

Multicomponent, selective self-assembly represents a unique assembly process, in which multiple varying components can selectively recognize and combine to generate only one discrete structure within a mixture.[7] Multicomponent selective self-assembly is a critical

zheng@chem.utah.edu, stang@chem.utah.edu.

phenomenon in many biological systems. Viral capsids such as *Tomato Bushy Stunt Virus* and *Rhinovirus*, for example, are assembled by three and four different subunits.[8] The proteasome of yeast *Saccharomyces Cerevisiae* is constructed from pairs of seven different proteins.[9] However, to obtain multicomponent selective self-assembly in an abiological system is a formidable challenge. By mixing various molecular components that lack sufficient complementary electronic and/or structural information, a self-organized mixture or even disordered oligomeric species can be formed instead of one finite, discrete supramolecule.[10] How to provide sufficient molecular information to control selective self-assembly in a multicomponent system remains a demanding issue in modern supramolecular chemistry.[6]

In the area of coordination-driven self-assembly, several methods have been developed to achieve multicomponent, selective self-assembly. Sauvage[11] and Lehn,12 in a pioneering study, used topological information to guide the selective self-assembly of multicomponent pseudorotaxanes. Recently, it was found that steric constraint could be exploited to control the multicomponent selective self-assembly, as evidenced by the impressive examples of Schmittel,13 Fujita,14 and Kobayashi.[15] However, the incorporation of topological or steric information into molecular components requires significant synthetic effort. Fujita demonstrated the facile selective self-assembly of 3-D trigonal prisms by mixing Palladium (II) acceptors with di- and trioptic pyridyl ligands, but a template is essential for the self-assembly.[16]

Recently, we demonstrated the facile selective self-assembly of multicomponent 2-D fused polygons and 3-D tetragonal prisms,[17] and both were achieved just by mixing suitable directional organoplatinum acceptors and different pyridyl donors without templates. These assemblies rely mainly on the stoichiometry and directionality of the molecular components, and are controlled by maximum site occupancy and entropy. To further extend the scope of facile, selective self-assembly and the diversity of multicomponent coordination-driven self-assembly, herein we present a multicomponent approach using the coordination-driven self-assembly of a 90° Pt(II) acceptor with pyridyl and carboxylate ligands. With suitable stoichiometry and geometries of the molecular binding units, 2-D supramolecular rectangles (Scheme 1) and 3-D prisms (Scheme 2) can be obtained selectively from multicomponent mixtures, due to the lower energy of the heteroleptic system, as shown in Scheme 3. The products were characterized via ^{31}P and ^{1}H multinuclear NMR spectroscopy, electrospray ionization (ESI) mass spectrometry, and pulsed-field-gradient spin-echo (PGSE) NMR measurements together with computational simulations. In addition, a porphyrin tetragonal prism constructed by this method demonstrated the ability to encapsulate triphenylene in an aqueous acetone solution.

Furthermore, this selective self-assembly can be achieved not only by the assembly of the individual molecular components, but also via supramolecule-to-supramolecule transformations. Supramolecular transformations have been reported that rely on triggering of the molecular subunits by light, solvent variation, or chemical signals,[18] but this phenomenon is rarely observed in a selective self-assembly system.[19] We investigated supramolecular transformations in multicomponent selective self-assembly as shown in Scheme 4, where 90° Pt(II) acceptors and pyridyl ligands self-assemble into well-defined homoleptic[6] supramolecular structures. Addition of a neutral triangle, assembled by the 90° Pt(II) acceptor and the carboxylate ligand, to the pyridyl-based square results in conversion of the homoleptic structures into a single, multicomponent heteroleptic6 supramolecule of different topology. These supramolecular transformation processes may be monitored by ^{31}P and ^{1}H multinuclear NMR spectroscopy.

Results and Discussions

Selective self-assembly of a multicomponent supramolecular rectangle

Cis-$Pt(PEt_3)_2(OTf)_2$ **1** was mixed with dicarboxylate ligand **2** and linear dipyridyl donor **3** in a 2:1:1 ratio, followed by addition of D_2O and Acetone-d_6. After 3h of heating at 75 °C, all solvent was removed from the clear solution, and Acetone-d_6 was then added into the mixture. A clear solution was afforded after an additional 5 h of heating at 75 °C, containing the supramolecular rectangle **4** as shown in Scheme 1. ^{31}P and ^{1}H multinuclear NMR spectroscopy and ESI mass spectrometry were used to characterize **4**.

In the $^{31}P\{^{1}H\}$ NMR spectrum (Figure 1b), two coupled doublets at 6.60 ppm and 1.06 ppm ($^{2}J_{P\text{-}P}$ = 22.0 Hz) of approximately equal intensity with concomitant ^{195}Pt satellites were found, indicating that the Pt(II) centers of **4** bear a heteroleptic coordination motif with pyridyl and carboxylate moieties.[20] The doublet at 1.06 ppm is shifted approximately 12 ppm upfield relative to **1** (Figure 1a) upon coordination, and corresponds to the phosphorous nuclei *trans* to the pyridine ring, while the doublet at 6.60 ppm is due to the phosphorous nuclei opposite to the carboxylate group.20a–c The two signals are coupled, indicating that chemically inequivalent phosphorous nuclei are bound to the same Pt(II) center, consistent with the heteroleptic coordination motif of rectangle **4**. In the ^{1}H NMR spectrum (Figure S1 in the Supporting Information), signals corresponding to the coordinated pyridine and carboxylate ligands were identified at 9.00 ppm ($H_{\alpha\text{-}Py}$), 7.74 ppm ($H_{\beta\text{-}Py}$), and 7.66 ppm (H_{phenyl}). The sharp and identifiable signals in both the $^{31}P\{^{1}H\}$ and ^{1}H NMR spectra support the self-assembly of the highly symmetric rectangle **4** as the predominant product in the mixture, and rule out the formation homoleptic assemblies or oligomers. ESI mass spectrometry further confirms the formation of a [4+2+2] multicomponent supramolecular rectangle **4**. In Figure 2, peaks attributable to **4** with lose of two and three triflate anions can be observed at *m/z* = 1455.69 ($[M - 2OTf]^{2+}$) and *m/z* = 920.88 ($[M - 3OTf]^{3+}$). All these peaks are isotopically resolved and in good agreement with the theoretical distribution.

Selective self-assembly of multicomponent supramolecular prisms

To date, the selective self-assembly of 3-D supramolecules have always required a template, 16 and are rarely obtained based solely on the intrinsic information of the complementary subunits.[13] Herein, we report the selective self-assembly of 3-D supramolecular prisms by mixing a 90° Pt(II) acceptor, a carboxylate ligand, and different multi-pyridyl ligands, as shown in Scheme 2.

Upon mixing 90° Pt(II) acceptor **1** and carboxylate ligand **2** with tri- or tetrapyridyl donors **5** or **6** in a specific ratio (for **7**: **1**:**2**:**5** = 6:3:2; for **8**: **1**:**2**:**6** = 8:4:2), supramolecular prisms **7** and **8** were formed as the predominant species, after equilibration. The $^{31}P\{^{1}H\}$ NMR spectra (Figure 3) of **7** and **8** are dominated by two coupled doublets (**7**: 6.56 ppm and 1.01 ppm, $^{2}J_{P\text{-}P}$ = 22.0 Hz; **8a**: 5.88 ppm and 1.08 ppm, $^{2}J_{P\text{-}P}$ = 21.4 Hz; **8b**: 5.07 ppm and −0.34 ppm, $^{2}J_{P\text{-}P}$ = 21.4 Hz) of similar intensity with concomitant ^{195}Pt satellites. These data, as expected, support the heteroleptic coordination environments of supramolecular prisms **7** and **8**, and rule out the formation of homoleptic complexes or oligomers. Likewise, in the ^{1}H NMR spectra (Figure S2-4 in Supporting Information), signals attributable to the coordinated pyridyl and carboxylate moieties are observed for **7**: 9.02 ppm ($H_{\alpha\text{-}Py}$), 7.75 ppm ($H_{\beta\text{-}Py}$), 7.77 ppm (H_{phenyl}); for **8a**: 8.87 ppm ($H_{\alpha\text{-}Py}$), 7.89 ppm ($H_{\beta\text{-}Py}$), 7.60 ppm (H_{phenyl}); and for **8b**: 9.27 ppm ($H_{\alpha\text{-}Py}$), 8.34 ppm ($H_{\beta\text{-}Py}$), 8.09 ppm (H_{phenyl}). The sharp signals in both the $^{31}P\{^{1}H\}$ and ^{1}H NMR spectra support the predominant formation of highly symmetric supramolecules **7** and **8**.

While suitable X-ray-quality crystals were not obtained, a computational study (see Supporting Information) together with PGSE NMR measurements was carried out to gain

insight into the structural parameters of these assemblies.[21] A molecular dynamics simulation using Maestro and Macromodel with a MMFF or MM2* force field, at 300K, in the gas phase was applied to equilibrate each supramolecule, and the output of the simulation was then minimized to full convergence. As shown in Figure 5, models of assemblies **7** and **8** have the shape of a trigonal and tetragonal prisms, respectively, with radii of 12 ε (**7**), 13 ε (**8a**), and 12 ε (**8b**). PGSE NMR experiments were carried out to measure the hydrodynamic radius for these assemblies and the results from these measurements agree with those from the modeled structures: 12.1 ± 0.1 ε (**7**), 11.6 ± 0.3 ε (**8a**), and 10.9 ± 0.1 ε (**8b**).

The multinuclear (^{31}P and ^{1}H) NMR spectroscopy, ESI mass spectrometry, and PGSE NMR measurements, along with the computational simulations, clearly support the selective self-assembly of heteroleptic 2-D and 3-D multicomponent supramolecules **4**, **7**, and **8**. To achieve a quantitative insight into such selective multicomponent self-assembly, a computational study has been performed to estimate the energy preference between the homoleptic and heteroleptic systems. To reduce redundancy and maintain accuracy, a simplified model system was used, as shown in Scheme 3, involving only two 90° acceptors, two pyridine (Py), and two benzoate anions ($C_7H_5O_2^-$). Upon heteroleptic coordination (the bottom route in Scheme 3), two heteroleptic molecules *cis*-$Pt(PEt_3)_2PyC_7H_5O_2^+$ may be formed, whereas the top route in Scheme 3 results in the formation of homoleptic species *cis*-$Pt(PEt_3)_2Py_2^{2+}$ and *cis*-$Pt(PEt_3)_2(C_7H_5O_2)_2$. Computational simulations (MMFF force field, gas phase, 300 K) for these heteroleptic and homoleptic species were carried out using Maestro and Macromodel. According to MMFF computational results (see Supporting Information), the energy of the system containing two heteroleptic molecules *cis*-$Pt(PEt_3)_2PyC_7H_5O_2^+$ is significantly lower than that with two homoleptic species (ΔE = −364.6 kJ/mol), and, therefore, the heteroleptic system is favored.

Well supported by both the experimental data and computational calculations, this selective self-assembly is solely driven by the intrinsic information of the molecular components, without involving a template or extra directing factors such as steric and topological constraints.[13-15] Presumably, the different electronic nature of carboxylate (negative) and pyridine (neutral) donor is a major driving factor, which allows for the heteroleptic coordination via charge separation. For example, in the simplified system illustrated in Scheme 3, within the homoleptic complex *cis*-$Pt(PEt_3)_2Py_2^{2+}$, two coordinated pyridyl moieties may be partially charged[22] and result in electrostatic repulsion between them. On the other hand, for the heteroleptic species *cis*-$Pt(PEt_3)_2PyC_7H_5O_2^+$, only one pyridyl moiety is coordinated to each Pt(II) center, and, therefore, the charges can be separated and the electrostatic repulsion can be reduced. Thus, the heteroleptic complex carries the lower energy. Additional experimental and computational studies are underway to further characterize the preference for heteroleptic complex formation. Understanding the factors driving these systems will allow optimization of this strategy for the formation of new multi-component assemblies.

Self-assembly via supramolecule-to-supramolecule transformations

Multicomponent, selective self-assembly can be achieved not only by the conventional assembly of individual molecular components, as described above, but also via supramolecule-to-supramolecule transformations. Supramolecular transformations may be defined as a process whereby a supramolecular species alters its structure (and composition) upon suitable external stimulus, such as photo, electrochemical, or chemical signals.[18] Here, we describe multicomponent selective self-assembly via supramolecular transformations from homoleptic to heteroleptic systems as shown in Scheme 4. The investigation was carried out by first preparing the homoleptic self-assemblies of 90° Pt(II) acceptor **1** with pyridyl ligands **3**, **4**, and **5b**, and then adding the neutral triangle **12** assembled by 90° Pt(II)

acceptor **1** and carboxylate ligand **2**. As a result, the pre-assembled homoleptic square **9**, truncated tetrahedron **10**, and trigonal prism **11** can be entirely transformed to the multicomponent heteroleptic rectangle **4**, trigonal prism **7**, and tetragonal prism **8b**, respectively.

The homoleptic ensembles **9**, **10**, and **11** as well as the neutral triangle **12** were obtained by mixing the 90° Pt(II) acceptor **1** with pyridyl ligands **3**, **4**, and **5b** and carboxylate donor **2**, respectively, in 1:1 (**9**), 3:2 (**10**), 2:1 (**11**), and 1:1 (**12**) ratios. Each structure was characterized by ^{31}P and ^{1}H multinuclear NMR spectroscopy, ESI mass spectrometry, and PGSE NMR measurements. In the ^{31}P{^{1}H} NMR spectra (Figure 6a-d), only one intense singlet (**9**: 0.36 ppm; **10**: 0.29 ppm; **11**: 0.90 ppm; **12**: 3.52 ppm) with concomitant ^{195}Pt satellites can be found. Likewise, the ^{1}H NMR spectra (Figure S7,9,11,14 in Supporting Information) show sharp signals assigned to the coordinated pyridyl moieties (e.g. δ = 9.28 ppm, $H_{α\text{-}Py}$ in **9**; δ = 9.32 ppm, $H_{α\text{-}Py}$ in **10**; δ = 9.75 ppm, $H_{α\text{-}Py}$ in **11**) and the carboxylate moieties (δ = 7.74 ppm in **12**). These NMR spectral results are in accord with the highly symmetric structure of **9**, **10**, **11**, and **12**. ESI mass spectrometry further confirms these assemblies (see Supporting Information). Signals for the [4 + 4] and [6 + 4] self-assembly of **9** and **10** can be found at m/z = 1869.91 [**9** – 2OTf]$^{2+}$, m/z = 1197.08 [**9** – 3OTf]$^{3+}$, m/z = 1818.36 [**10** – 3OTf]$^{3+}$, and m/z = 1326.65 [**10** – 4OTf]$^{4+}$. [6 + 3] Self-assembly of trigonal prism **11** was also supported by observation of isotopically resolved signals at m/z = 2966.57 [**11** – 2OTf]$^{2+}$, m/z = 1408.99 [**11** – 4OTf]$^{4+}$, and m/z = 1097.48 [**11** – 5OTf]$^{5+}$, but those for larger assemblies such as [4 + 4], [5 + 5], and [6 + 6] could not be found, ruling out the formation of larger prisms.[23] For the neutral triangle **12**, the molecular ion peak for the [3 + 3] self-assembly was found at m/z = 1787.12 [**12** + H]$^{+}$ and m/z = 1809.11 [**12** + Na]$^{+}$, along with the signal for [**12** + 2Na]$^{2+}$at m/z = 916.16. There is no molecular ion peak for [2 + 2] or [4 + 4] ensembles observed in the mass spectrum, excluding formation of a [2 + 2] rectangle or a [4 + 4] square. Furthermore, a PGSE NMR study was also carried out to estimate the size of the trigonal prism **11**, and the experimental radius obtained (1.70 ± 0.04 nm) is in good agreement with the computational value of 1.6 nm from MMFF modeling (Figure S13 in Supporting Information).[21]

The transformation of the homoleptic self-assemblies into the heteroleptic assemblies was carried out by the addition of a solution of the above homoleptic product to the neutral triangle **12**. After 5 h of heating at 75 °C, a clear solution was obtained and characterized by ^{31}P and ^{1}H multinuclear NMR spectroscopy. In the ^{31}P{^{1}H} NMR spectra (Figure 6e-g), two intense coupled doublet peaks (Figure 6e: 6.63 ppm and 1.08 ppm, $^{2}J_{P\text{-}P}$ = 22.0 Hz for **4**; Figure 6f: 6.63 ppm and 1.03 ppm, $^{2}J_{P\text{-}P}$ = 21.4 Hz for **7**; Figure 6g: 5.03 ppm and −0.35 ppm, $^{2}J_{P\text{-}P}$ = 21.4 Hz for **8b**) with concomitant ^{195}Pt satellites were found, which were in good agreement with those observed in Figure 1 and 3 for the authentic heteroleptic cages. Likewise, in the ^{1}H NMR spectra (Figure S16 in Supporting Information), the signals of the heteroleptic structures obtained by supramolecular transformation match the signals of the authentic ensembles. Peaks corresponding to the starting homoleptic structures were absent in both ^{31}P{^{1}H} and ^{1}H NMR spectra. These NMR data clearly indicate that the homoleptic assemblies have been entirely transformed into the multicomponent heteroleptic structures.

To further investigate the supramolecular transformation process, we carried out a study of the gradual transformation of square **9** to rectangle **4**: 10%, 25%, 50%, and 100% of neutral triangle **12** was added to an acetone solution of square **9**, and the mixtures were heated at 75 °C for 5 h. The resulting clear solutions were characterized by ^{31}P and ^{1}H multinuclear NMR spectroscopy. As indicated by the ^{31}P{^{1}H} NMR spectra (Figure 7), increasing the amount of **12** resulted in a decrease of the signal (δ = 0.36 ppm) for square **9** and the simultaneous formation of signals around 6.63 ppm and 0.99 ppm, attributable to heteroleptic complexes. A similar result can be observed in ^{1}H NMR spectra (Figure S17 in

Supporting Information) by comparing the signals for $H_{\alpha\text{-Py}}$ of the homoleptic assembly (δ = 9.28 ppm) and the heteroleptic complexes (δ = 9.00 ppm). These ^{31}P and ^{1}H NMR spectral results demonstrate the gradual transformation of heteroleptic complexes from the homoleptic species upon addition of the neutral triangle. During the transformation process, in addition to rectangle **4**, an intermediate was also observed, indicated by the multiplets around 6.63 ppm and 0.99 ppm in Figure 7b–d. Isotopically resolved signals in the ESI mass spectrum (see Supporting Information) at m/z = 722.56 $[M - 3OTf]^{3+}$ and 1158.25 $[M - 2OTf]^{2+}$ suggest this intermediate is formed by the [3 + 2 + 1] assembly of organoplatinum acceptor **1**, pyridyl donor **3**, and carboxylate ligand **2**, and these signals cannot be found in the spectrum of pure rectangle **4**, square **9**, or neutral triangle **12**. The intermediate is formed due to the improper ratio of square and neutral triangle for generating the [4 + 2 + 2] rectangle **4**. Once 100% of neutral triangle **12** was added, square **9** can be fully altered to rectangle **4** as indicated by Figure 7e and Figure S17e.

The Host-Guest Properties of the Multicomponent Structure

To explore potential applications of such multicomponent structures, a host-guest study was carried out as shown in Scheme 5: a multicomponent porphyrin cage soluble in aqueous acetone solution was prepared by the method described above, and then used as a host for encapsulating the aromatic guest, triphenylene. The multicomponent porphyrin cage **14** was prepared by mixing cis-$Pt(PMe_3)(OTf)_2$ (**13**) with tetrakis(4-pyridyl) porphyrin (**6b**) and sodium terephthalate (**2**) in a 4:1:2 ratio in an aqueous acetone solution (*v/v* 1:1). After heating at 85 °C for 24 h, a clear, purple solution was obtained. The $^{31}P\{^{1}H\}$ NMR spectrum (Figure S19 in the Supporting Information) of the solution shows two doublets at −24.3 ppm and −30.3 ppm of equal intensity with concomitant ^{195}Pt satellites. The ^{1}H NMR spectrum (Figure 8a), shows signals corresponding to coordinated pyridyl and carboxylate moieties, identified at 9.22 ppm ($H_{\alpha\text{-Py}}$), 8.28 ppm ($H_{\beta\text{-Py}}$), and 7.95 ppm (H_{phenyl}-**2**). The NMR spectral evidence clearly indicates that a heteroleptic ensemble was predominantly formed in the solution. Isotopically resolved signals in the ESI-MS spectrum at m/z = 1806.24 ([**14** – 3OTf]$^{3+}$) and m/z = 1317.69 ([**14** – 4OTf]$^{4+}$) (Figure S20 in the Supporting Information) further support that the heteroleptic species is the multicomponent porphyrin cage **14**.

The host-guest properties of **14** were studied by the addition of excess triphenylene (**TP**) in aqueous acetone solution to the cage. After heating at 85 °C for 16 h, the encapsulated complex was present in the mixture. Two doublets at −24.3 ppm −30.3 ppm with concomitant ^{195}Pt satellites in the $^{31}P\{^{1}H\}$ NMR spectrum (see Supporting Information) and the identifiable peaks (δ = 9.22 ppm for $H_{\alpha\text{-Py}}$, δ = 8.28 ppm for $H_{\beta\text{-Py}}$, and δ = 7.95 ppm for H_{phenyl}-**2**) in the ^{1}H NMR spectra (Figure 8c) indicated that the coordinative porphyrin cage structure was retained. By comparing the ^{1}H NMR spectra of pure **14** and **TP** with the mixture (Figure 8), shifted signals were observed at 8.11 ppm (Δδ = −0.54 ppm, $H_{\text{triphenylene}}$) and 7.26 ppm (Δδ = −0.38 ppm, $H_{\text{triphenylene}}$), indicating that the triphenylene **TP** was encapsulated in the porphyrin cage, **14**. The ESI mass spectra (Figure 9), showed isotopically resolved signals at m/z = 1373.91 [**14**·**TP** – 4OTf]$^{4+}$ and m/z = 1069.72 [**14**·**TP** – 5OTf]$^{5+}$ confirming that one triphneylene molecule **TP** was encapsulated in the cage of **14**. Integration of the proton NMR signals indicated that 27% of cage **14** contained guest molecules under these conditions.

A computational simulation was used to gain insight about the structural features of the encapsulated complex **14**·**TP**. A molecular dynamics simulation using MM2* force fields at 300K in the aqueous phase was used to equilibrate the complex, and the output of the simulation was then minimized to full convergence. As shown in Figure 10, one triphenylene molecule **TP** is trapped within the cavity of **14**, and the distance between the guest and porphyrin faces is about 3.8 Å.

Conclusion

We report here a facile and very efficient approach for the selective construction of well-defined multicomponent 2-D and 3-D supramolecular structures of various motifs. Upon combination of a 90° Pt(II) acceptor and a carboxylate ligand with appropriate pyridyl donors in a proper ratio, coordination-driven self-assembly allows for the selective formation of a multicomponent supramolecular rectangle and prisms. These multicomponent complexes can also be obtained by a novel supramolecule-to-supramolecule transformation from homoleptic assemblies. Characterization via multinuclear (^{31}P and ^{1}H) NMR spectroscopy clearly reveals the heteroleptic coordination nature of these assembled supramolecules, as well as their high structural symmetry. ESI mass spectrometry and PGSE NMR measurements, together with computational simulations, further identify the composition and size of these multicomponent assemblies. Presumably, such multicomponent, selective self-assembly processes are directed, in part, by a charge separation effect, whereby a negative carboxylate ligand and a neutral pyridyl donor favors a heteroleptic motif upon coordination with Pt(II) centers. These cage structures show a unique 3-D nanoscale pore, and preliminary studies indicate the nano-cavity is able to encapsulate triphenylene. These selectively self-assembled multicomponent supramolecules can be further developed into functionalized scaffolds via pre/post-modifications, which is currently under investigation.

Experimental Section

Methods and Materials

Molecular building blocks **1**[24], **3**[25], **5**[26], and **6a**[17b] were prepared according to literature procedures. Carboxylate ligand **2** was prepared by neutralization of terephthalic acid with 2 equiv. NaOH. All other reagents were purchased from Aldrich or Alfa and used without further purification. Deuterated solvents were purchased from Cambridge Isotope Laboratory (Andover, MA). Multinuclear (^{31}P and ^{1}H) NMR spectra were recorded on a Varian Unity 300 spectrometer, and PGSE NMR data were obtained on an Inova 500 MHz spectrometer. Mass spectra were recorded on a Micromass Quattro II triple-quadrupole mass spectrometer using electrospray ionization with a MassLynx operating system. Element analysis was performed by Atlantic Microlab (Norcross, GA).

General procedure for selective self-assembly

Cis-Pt(PEt_3)$_2$(OTf)$_2$ **1**, carboxylate ligand **2**, and various pyridyl donors were placed in a 2-dram vial, followed by addition of D_2O (0.2 mL) and Acetone-d_6 (0.8 mL). After 3 h of heating at 75 °C, all solvent was removed by N_2 flow, and then dried under vacuum. Acetone-d_6 (0.7 mL) was then added into each mixture. A clear solution was obtained after an additional 5 h of heating at 75 °C. The resulted multicomponent supramolecules were isolated via precipitation by addition of Et_2O or KPF_6.

Synthesis and Characteristics of 4

Reaction scale: *Cis*-Pt(PEt_3)$_2$(OTf)$_2$ **1** (5.37 mg, 7.36 μmol), carboxylate ligand **2** (0.77 mg, 3.7 μmol), and ditopic pyridyl ligand **3** (1.03 mg, 3.68 μmol). Yield: 90%. MS (ESI) calcd for [M – 2OTf]$^{2+}$ *m/z* 1455.85, found 1455.69; calcd for [M – 3OTf]$^{3+}$ *m/z* 920.92, found 920.88. ^{1}H NMR (Acetone-d_6, 300MHz) δ 9.00 (s, 8H, $H_{\alpha\text{-Py}}$), 7.74 (m, 16H, $H_{\beta\text{-Py}}$ and $H_{\text{phenyl-Py}}$), 7,66 (s, 8H, H_{phneyl}), 1.92 (m, 48H, PCH_2CH_3), 1.21 (m, 72H, PCH_2CH_3). ^{31}P{^{1}H} NMR (Acetone-d_6, 121.4 MHz) δ 6.60 (d, $^{2}J_{\text{P-P}}$ = 22.0 Hz, ^{195}Pt satellites, $^{1}J_{\text{Pt-P}}$ = 3242 Hz), 1.06 (d, $^{2}J_{\text{P-P}}$ = 22.0 Hz, ^{195}Pt satellites, $^{1}J_{\text{Pt-P}}$ = 3427 Hz). Anal. Calcd for $C_{108}H_{152}F_{12}N_4O_{20}P_8Pt_4S_4$: C, 40.40; H, 4.77; N, 1.74. Found: C, 40.04; H, 4.70; N, 1.71.

Synthesis and Characteristics of 7

Reaction scale: *Cis*-$Pt(PEt_3)_2(OTf)_2$ **1** (4.88 mg, 6.69 μmol), carboxylate ligand **2** (0.71 mg, 3.4 μmol), and tritopic pyridyl ligand **5** (0.84 mg, 2.2 μmol). Yield: 91%. MS (ESI) calcd for $[M - 2OTf]^{2+}$ *m/z* 2218.98, found 2218.76; calcd for $[M - 3OTf]^{3+}$ *m/z* 1429.67, found 1429.59. ^1H NMR (Acetone-d_6, 300MHz) δ 9.02 (s, 12H, $H_{α\text{-}Py}$), 7,88 (s, 12H, $H_{phneyl\text{-}Py}$), 7.75 (m, 24H, $H_{β\text{-}Py}$ and H_{phenyl}), 1.89 (m, 72H, PCH_2CH_3), 1.20 (m, 108H, PCH_2CH_3). $^{31}P\{^1H\}$ NMR (Acetone-d_6, 121.4 MHz) δ 6.56 (d, $^2J_{P\text{-}P}$ = 22.0 Hz, ^{195}Pt satellites, $^1J_{Pt\text{-}P}$ = 3227 Hz), 1.01 (d, $^2J_{P\text{-}P}$ = 22.0 Hz, ^{195}Pt satellites, $^1J_{Pt\text{-}P}$ = 3404 Hz). Anal. Calcd for $C_{156}H_{222}F_{18}N_6O_{30}P_{12}Pt_6S_6$: C, 39.55; H, 4.72; N, 1.77. Found: C, 39.92; H, 4.54; N, 1.79.

Synthesis and Characteristics of 8a

Reaction scale: *Cis*-$Pt(PEt_3)_2(OTf)_2$ **1** (5.22 mg, 7.16 μmol), carboxylate ligand **2** (0.75 mg, 3.6 μmol), and tetratopic pyridyl ligand **6a** (1.14 mg, 1.78 μmol). Yield: 96%. MS (ESI) calcd for $[M - 3PF_6]^{3+}$ *m/z* 2037.86, found 2037.75; calcd for $[M - 5PF_6]^{5+}$ *m/z* 1164.51, found 1164.50. ^1H NMR (Acetone-d_6, 300MHz) δ 8.87 (s, 16H, $H_{α\text{-}Py}$), 7,89 (d, *J* = 6 Hz, 16H, $H_{α\text{-}phneylPy}$), 7.60 (m, 32H, $H_{β\text{-}Py}$ and H_{phenyl}), 7,20 (d, *J* = 6 Hz, 16H, $H_{β\text{-}phneyl\text{-}Py}$), 1.89 (m, 96H, PCH_2CH_3), 1.17 (m, 144H, PCH_2CH_3). $^{31}P\{^1H\}$ NMR (Acetone-d_6, 121.4 MHz) δ 5.88 (d, $^2J_{P\text{-}P}$ = 21.4 Hz, ^{195}Pt satellites, $^1J_{Pt\text{-}P}$ = 3270 Hz), 1.08 (d, $^2J_{P\text{-}P}$ = 21.4 Hz, ^{195}Pt satellites, $^1J_{Pt\text{-}P}$ = 3448 Hz). Anal. Calcd for $C_{220}H_{320}F_{48}N_8O_{16}P_{24}Pt_8$: C, 40.35; H, 4.93; N, 1.71. Found: C, 40.71; H, 5.08; N, 1.74.

Synthesis and Characteristics of 8b

Reaction scale: *Cis*-$Pt(PEt_3)_2(OTf)_2$ **1** (4.52 mg, 6.10 μmol), carboxylate ligand **2** (0.63 mg, 3.0 μmol), and tetratopic pyridyl ligand **6b** (0.94 mg, 1.5 μmol). Yield: 95%. MS (ESI) calcd for $[M - 3PF_6]^{3+}$ *m/z* 2022.83, found 2022.71; calcd for $[M - 5PF_6]^{5+}$ *m/z* 1155.71, found 1155.62. ^1H NMR (CD_3NO_2, 300MHz) δ 9.27 (m, 24H, $H_{α\text{-}Py}$ and $H_{Pyrrole}$), 8.34 (d, *J* = 5.7 Hz, 16H, $H_{β\text{-}Py}$), 8.08 (s, 16H, H_{phneyl}), 7.12 (s, 8H, $H_{Pyrrole}$), 2.24 (m, 96H, PCH_2CH_3), 1.39 (m, 144H, PCH_2CH_3). −3.28 (s, 4H, $H_{N\text{-}H}$). $^{31}P\{^1H\}$ NMR (CD_3NO_2, 121.4 MHz) δ 5.07 (d, $^2J_{P\text{-}P}$ = 21.4 Hz, ^{195}Pt satellites, $^1J_{Pt\text{-}P}$ = 3270 Hz), −0.34 (d, $^2J_{P\text{-}P}$ = 21.4 Hz, ^{195}Pt satellites, $^1J_{Pt\text{-}P}$ = 3462 Hz). Anal. Calcd for $C_{208}H_{308}F_{48}N_{16}O_{16}P_{24}Pt_8$: C, 38.41; H, 4.77; N, 3.45. Found: C, 38.07; H, 4.92; N, 3.41.

Self-Assembly of 9

Cis-$Pt(PEt_3)_2(OTf)_2$ **1** (5.07 mg, 6.95 μmol) and ditopic pyridyl ligand **3** (1.95 mg, 6.96 μmol) were placed in a 2-dram vial, followed by addition of 0.7 mL Acetone-d_6, which was then sealed with Teflon tape and immersed in an oil bath at 70 °C for 2 h. Solid product was obtained by removing the solvent under vacuum. Yield: 97%. MS (ESI) calcd for $[M - 2OTf]^{2+}$ *m/z* 1869.84, found 1869.91; calcd for $[M - 3OTf]^{3+}$ *m/z* 1197.25, found 1197.08. ^1H NMR (Acetone-d_6, 300MHz) δ 9.28 (d, *J* = 4.8 Hz, 16H, $H_{α\text{-}Py}$), 7.79 (d, *J* = 6.0 Hz, 16H, $H_{β\text{-}Py}$), 7.69 (s, 16H, $H_{phneyl\text{-}Py}$), 2.08 (m, 48H, PCH_2CH_3), 1.29 (m, 72H, PCH_2CH_3). $^{31}P\{^1H\}$ NMR (Acetone-d_6, 121.4 MHz) δ 0.36 (s, ^{195}Pt satellites, $^1J_{Pt\text{-}P}$ = 3099 Hz). Anal. Calcd for $C_{136}H_{168}F_{24}N_8O_{24}P_8Pt_4S_8$: C, 40.44; H, 4.19; N, 2.77. Found: C, 40.65; H, 4.21; N, 2.64.

Self-Assembly of 10

Cis-$Pt(PEt_3)_2(OTf)_2$ **1** (4.51 mg, 6.18 μmol) and tritopic pyridyl ligand **5** (1.55 mg, 4.06 μmol) were placed in a 2-dram vial, followed by addition of 0.7 mL Acetone-d_6, which was then sealed with Teflon tape and immersed in an oil bath at 70 °C for 2 h. Solid product was obtained by removing the solvent under vacuum. Yield: 98%. MS (ESI) calcd for $[M - 3OTf]^{3+}$ *m/z* 1818.32, found 1818.36; calcd for $[M - 4OTf]^{4+}$ *m/z* 1326.75, found

1326.65. ^{1}H NMR (Acetone-d_6, 300MHz) δ 9.32 (d, J = 4.8 Hz, 24H, $H_{α\text{-}Py}$), 8.04 (s, 12H, $H_{phneyl\text{-}Py}$), 7.83 (d, J = 6.3 Hz, 24H, $H_{β\text{-}Py}$), 2.09 (m, 72H, PCH_2CH_3), 1.29 (m, 108H, PCH_2CH_3). ^{31}P{^{1}H} NMR (Acetone-d_6, 121.4 MHz) δ 0.29 (s, ^{195}Pt satellites, $^{1}J_{Pt\text{-}P}$ = 3083 Hz). Anal. Calcd for $C_{192}H_{240}F_{36}N_{12}O_{36}P_{12}Pt_6S_{12}$: C, 39.07; H, 4.10; N, 2.85. Found: C, 39.25; H, 4.18; N, 2.81.

Self-Assembly of 11

To a 1.2 mL CD_2Cl_2 suspension of tetratopic pyridyl ligand **6b** (2.46 mg, 3.97 μmol) was added a 0.4 mL CD_3NO_2 solution of *Cis*-Pt$(PEt_3)_2(OTf)_2$ **1** (5.89 mg, 8.07 μmol), drop by drop, with continuous stirring (5 min). The reaction mixture was stirred at room temperature for 1 h, and then heated up to 70 °C for overnight. The solution was evaporated to dryness, and the product was collected. Yield: 98%. MS (ESI) calcd for $[M – 2OTf]^{2+}$ *m/z* 2966.54, found 2966.57; calcd for $[M – 4OTf]^{4+}$ *m/z* 1409.04, found 1408.99; calcd for $[M – 5OTf]^{5+}$ *m/z* 1097.44, found 1097.48. ^{1}H NMR (CD_2Cl_2/CD_3NO_2: 3/1, 300MHz) δ 9.75 (dd, J_1 = 4.8 Hz and J_2 = 36 Hz, 24H, $H_{α\text{-}Py}$), 8.98 (m, 36H, $H_{βPy}$ and $H_{Pyrrole}$), 8.51 (s, 12H, $H_{Pyrrole}$), 2.32 (m, 72H, PCH_2CH_3), 1.60 (m, 108H, PCH_2CH_3). ^{31}P{^{1}H} NMR (CD_2Cl_2/CD_3NO_2: 3/1, 121.4 MHz) δ 0.90 (s, ^{195}Pt satellites, $^{1}J_{Pt\text{-}P}$ = 3070 Hz). Anal. Calcd for $C_{204}H_{258}F_{36}N_{24}O_{36}P_{12}Pt_6S_{12}$: C, 39.31; H, 4.17; N, 5.39. Found: C, 39.83; H, 4.35; N, 5.16.

Self-Assembly of 12

Cis-Pt$(PEt_3)_2(OTf)_2$ **1** (2.12 mg, 2.91 μmol) and carboxylate ligand **2** (0.61 mg, 2.9 μmol) were placed in a 2-dram vial, followed by addition of 0.08 mL H_2O and 0.8 Acetone, which was then sealed with Teflon tape and immersed in an oil bath at 70 °C for 2 h. The solvent was then removed by N_2 flow, and the solid mixture was dried under vacuum. 0.6 mL Acetone-d_6 was added to the dried mixture and after 4 h of heating at 70 °C, the neutral triangle was formed. MS (ESI) calcd for $[M + H]^{+}$ *m/z* 1787.38, found 1787.12; calcd for $[M + Na]^{+}$ *m/z* 1809.47, found 1809.11; calcd for $[M + 2Na]^{2+}$ *m/z* 916.23, found 916.16. ^{1}H NMR (Acetone-d_6, 300MHz) δ 7.74 (s, 12H, H_{Phenyl}), 2.00 (m, 36H, PCH_2CH_3), 1.23 (m, 54H, PCH_2CH_3). ^{31}P{^{1}H} NMR (Acetone-d_6, 121.4 MHz) δ 3.52 (s, ^{195}Pt satellites, $^{1}J_{Pt\text{-}P}$ = 3619 Hz).

Self-Assembly of 14

Cis-Pt$(PMe_3)_2(OTf)_2$ **13** (3.92 mg, 5.38 μmol), carboxylate ligand **2** (0.56 mg, 2.67 μmol), and tetratopic pyridyl ligand **6b** (0.82 mg, 1.3 μmol) were placed in a 2-dram vial, followed by addition of 0.6 mL D_2O and 0.6 Acetone-d_6, which was then sealed with Teflon tape and immersed in an oil bath at 85 °C for 24 h. The multicomponent porphyrin cage 14 was formed. The solid product can be isolated by ion exchange with KPF_6. Yield: 95%. MS (ESI) calcd for $[M – 4OTf]^{4+}$ *m/z* 1317.69, found 1317.69; calcd for $[M – 3OTf]^{3+}$ *m/z* 1806.23, found 1806.24. ^{1}H NMR (D_2O/Acetone-d_6: 1/1, 300MHz) δ 9.22 (m, 24H, $H_{α\text{-}Py}$ and $H_{Pyrrole}$), 8.28 (d, J = 5.7 Hz, 16H, $H_{β\text{-}Py}$), 7.95 (s, 16H, H_{phneyl}), 6.96 (s, 8H, $H_{Pyrrole}$), 1.95 (d, J = 12 Hz, 72H, PCH_3), 1.80 (d, J = 12 Hz, 72H, PCH_3). ^{31}P{^{1}H} NMR (D_2O/Acetone-d_6: 1/1, 121.4 MHz) δ −24.3 (d, $^{2}J_{P\text{-}P}$ = 23.8 Hz, ^{195}Pt satellites, $^{1}J_{Pt\text{-}P}$ = 3324 Hz), −30.3 (d, $^{2}J_{P\text{-}P}$ = 23.8 Hz, ^{195}Pt satellites, $^{1}J_{Pt\text{-}P}$ = 3496 Hz). Anal. Calcd for $C_{160}H_{212}F_{48}N_{16}O_{16}P_{24}Pt_8$: C, 32.95; H, 3.66; N, 3.84. Found: C, 33.16; H, 3.60; N, 3.74.

Supplementary Material

Refer to Web version on PubMed Central for supplementary material.

Acknowledgments

P.J.S. thanks the NIH (Grant GM-057052) for financial support.

REFERENCES

1. a Stang PJ, Olenyuk B. Acc. Chem. Res 1997;30:502. b Leininger S, Olenyuk B, Stang PJ. Chem. Rev 2000;100:853. [PubMed: 11749254] c Holliday BJ, Mirkin CA. Angew. Chem., Int. Ed 2001;40:2022. d Fujita M, Umemoto K, Yoshizawa M, Fujita N, Kusukawa T, Biradha K. Chem. Commun 2001:509. e Seidel SR, Stang PJ. Acc. Chem. Res 2002;35:972. [PubMed: 12437322] f Ruben M, Rojo J, Romero-Salguero FJ, Uppadine LH, Lehn J-M. Angew. Chem., Int. Ed 2004;43:3644. (b). g Fiedler D, Leung DH, Bergman RG, Raymond KN. Acc. Chem. Res 2005;38:351. h Fujita M, Tominaga M, Hori A, Therrien B. Acc. Chem. Res 2005;38:369. [PubMed: 15835883] i Lukin O, Voegtle F. Angew. Chem., Int. Ed 2005;44:1456. j Severin K. Chem. Commun 2006:3859. k Nitschke JR. Acc. Chem. Res 2007;40:103. [PubMed: 17309191] l Pitt MA, Johnson DW. Chem. Soc. Rev 2007;36:1441. [PubMed: 17660877] m Oliver CG, Ulman PA, Wiester MJ, Mirkin CA. Acc. Chem. Res 2008;41:1618. [PubMed: 18642933] n Parkash MJ, Lah MS. Chem. Commun 2009:3326.

2. a Yang H-B, Das N, Huang F, Hawkridge AM, Muddiman DC, Stang PJ. J. Am. Chem. Soc 2006;128:10014. [PubMed: 16881621] b Yang H-B, Hawkridge AM, Huang SD, Das N, Bunge SD, Muddiman DC, Stang PJ. J. Am. Chem. Soc 2007;129:2120. [PubMed: 17256935] c Baytekin HT, Sahre M, Rang A, Engeser M, Schulz A, Schalley CA. Small 2008;4:1823. [PubMed: 18752209] d Yang H-B, Northrop BH, Zheng Y-R, Ghosh K, Lyndon MM, Muddiman DC, Stang PJ. J. Org. Chem 2009;74:3524. [PubMed: 19344131] e Yang H-B, Northrop BH, Zheng Y-R, Ghosh K, Stang PJ. J. Org. Chem 2009;74:7067. [PubMed: 19691266] f Zheng Y-R, Ghosh K, Yang H-B, Stang PJ. Inorg. Chem 2010;49:4747. [PubMed: 20443570]

3. a Pluth MD, Bergman RG, Raymond KN. J. Am. Chem. Soc 2008;130:6362. [PubMed: 18444618] b Klosterman JK, Yamauchi Y, Fujita M. Chem. Soc. Rev 2009;38:1714. [PubMed: 19587964] c Yamauchia Y, Yoshizawa M, Akita M, Fujita M. Prod. Nat. Acd. Sci. USA 2009;106:10435. d Hatakeyama Y, Sawada T, Kawano M, Fujita M. Angew. Chem., Int. Ed 2009;48:8695. e Pluth MD, Fiedler D, Mugridge JS, Bergman RG, Raymond KN. Prod. Nat. Acd. Sci. USA 2009;106:10438. f Mal P, Breiner B, Rissanen K, Nitschke JR. Science 2009;324:1697. [PubMed: 19556504] g Sawada T, Fujita M. J. Am. Chem. Soc 2010;132:7194. [PubMed: 20429562]

4. a Yoshizawa M, Tamura M, Fujita M. Science 2006;312:251. [PubMed: 16614218] b Pluth, Michael D, Bergman, Robert G, Raymond, Kenneth N. Science 2007;316:85. [PubMed: 17412953] c Pluth MD, Bergman RG, Raymond KN. Acc. Chem. Res 2009;42:1650. [PubMed: 19591461] d Yoshizawa M, Klosterman JK, Fujita M. Angew. Chem., Int. Ed 2009;48:3418.

5. a Yamashita K-I, Kawano M, Fujita M. Chem. Commun 2007;40:4102. b Lee SJ, Lin W. Acc. Chem. Res 2008;41:521. [PubMed: 18271561] c Steed JW. Chem. Soc. Rev 2009;38:506. [PubMed: 19169464] d Liu Y, Wu X, He C, Jiao Y, Duan C. Chem. Commun 2009;48:7554.

6. De S, Mahata K, Schmittel M. Chem. Soc. Rev 2010;39:1555. [PubMed: 20419210]

7. a Lehn J-M. Science 2002;295:2400. [PubMed: 11923524] b Lehn J-M. Rep. Prog. Phys 2004;67:249. c Lehn J-M. Chem. Soc. Rev 2008;36:151. [PubMed: 17264919]

8. a Abad-Zapatero C, Abdel-Meguid SS, Johnson JE, Leslie AGW, Rayment I, Rossmann MG, Suck D, Tsukihara T. Nature 1980;286:33. [PubMed: 19711553] b Rossmann MG, Arnold E, Erickson JW, Frankenberger EA, Griffith JP, Hecht HJ, Johnson JE, Kamer G, Luo M, Mosser AG, Mosser AG, Rueckert RR, Sherry B, Vriend G. Nature 1985;317:145. [PubMed: 2993920]

9. Groll M, Dizel L, Lowe J, Stock D, Bochter M, Bartunik HD, Huber R. Nature 1997;386:463. [PubMed: 9087403]

10. a Zheng Y-R, Yang H-B, Northrop BH, Ghosh K, Stang PJ. Inorg. Chem 2008;47:4706. [PubMed: 18433099] b Northrop BH, Yang H-B, Stang PJ. Inorg. Chem 2008;47:11257. [PubMed: 18980302] c Northrop BH, Zheng Y-R, Chi K-W, Stang PJ. Acc. Chem. Res 2009;42:1554. [PubMed: 19555073] d Zheng Y-R, Yang H-B, Ghosh K, Zhao L, Stang PJ. Chem. Eur. J 2009;15:7203.

11. a Sauvage J-P, Weiss J. J. Am. Chem. Soc 1985;107:6108. b Nierengarten JF, Dietrich-Buchecker CO, Sauvage J-P. J. Am. Chem. Soc 1994;116:375. c Amabilino DA, Dietrich-Buchecker CO, Sauvage J-P. J. Am. Chem. Soc 1996;118:3285. d Solladié N, Chambron J-C, Sauvage J-P. J. Am. Chem. Soc 1999;121:3684.
12. Sleiman H, Baxter P, Lehn J-M, Rissanen K. J. Chem. Soc., Chem. Commun 1995:715.
13. a Schmittel M, Ganz A. Chem. Commun 1997:999. b Schmittel M, Ganz A, Fenske D. Org. Lett 2002;4:2289. [PubMed: 12098229] c Schmittel M, Ammon H, Kalsani V, Wiegrefe A, Michel C. Chem. Commun 2002:2566. d Schmittel M, Kalsani V, Fenske D, Wiegrefe A. Chem. Commun 2004;5:490. e Schmittel M, Kalsani V, Bats JW. Inorg. Chem 2005;44:4115. [PubMed: 15934731] f Schmittel M, Mahata K. Angew. Chem., Int. Ed 2008;47:5284. g Schmittel M, Mahata K. Inorg. Chem 2009;48:822. [PubMed: 19128046] h Fan J, Bats JW, Schmittel M. Inorg. Chem 2009;48:6338. [PubMed: 19527007] i Mahata K, Schmittel M. J. Am. Chem. Soc 2009;131:16544. [PubMed: 19860466]
14. a Yoshizawa M, Nagao M, Kumazawa K, Fujita M. J. Organomet. Chem 2005;690:5383. b Yamauchi Y, Fujita M. Chem. Commun 2010;46:5897.
15. Yamanaka M, Yamada Y, Sei Y, Yamaguchi K, Kobayashi K. J. Am. Chem. Soc 2006;128:1531. [PubMed: 16448123]
16. a Kumazawa K, Biradha K, Kusukawa T, Okano T, Fujita M. Angew. Chem., Int. Ed 2003;42:3909. b Yoshizawa M, Nakagawa J, Kurnazawa K, Nagao M, Kawano M, Ozeki T, Fujita M. Angew. Chem., Int. Ed 2005;44:1810.
17. a Lee J, Ghosh K, Stang PJ. J. Am. Chem. Soc 2009;131:12028. [PubMed: 19663439] b Wang M, Zheng Y-R, Ghosh K, Stang PJ. J. Am. Chem. Soc 2010;132:6282. [PubMed: 20405914]
18. a Sun S-S, Anspach JA, Lees AJ. Inorg. Chem 2002;41:1862. [PubMed: 11925181] b Sun S-S, Stern CL, Nguyen ST, Hupp JT. J. Am. Chem. Soc 2004;126:6314. [PubMed: 15149229] c Heo J, Jeon Y-M, Mirkin CA. J. Am. Chem. Soc 2007;129:7712. [PubMed: 17539639] d Zhao L, Northrop BH, Stang PJ. J. Am. Chem. Soc 2008;130:11886. [PubMed: 18702485]
19. Campbell VE, Hatten X, Delsuc N, Kauffmann B, Huc I, Nitschke JR. Nature Chem 2010;2:684. [PubMed: 20651733]
20. a Chi K-W, Addicott C, Arif AM, Stang PJ. J. Am. Chem. Soc 2004;126:16569. [PubMed: 15600362] b Chi K-W, Addicott C, Kryschenko YK, Stang PJ. J. Org. Chem 2004;69:964. [PubMed: 14750829] c Chi K-W, Addicott C, Moon M-E, Lee HJ, Yoon SC, Stang PJ. J. Org. Chem 2006;71:6662. [PubMed: 16901167] d Ghosh S, Turner DR, Batten SR, Mukherjee PS. Dalton Trans 2007:1869. [PubMed: 17702163]
21. Caskey DC, Yamamoto T, Addicott C, Shoemaker RK, Vacek J, Hawkridge AM, Muddiman DC, Kottas GS, Michl J, Stang PJ. J. Am. Chem. Soc 2008;130:7620. and references therein. [PubMed: 18491898]
22. Penka EF, Schläpfer CW, Atanasov M, Albrecht M, Daul C. J. Organomet. Chem 2007;692:5709.
23. Bar AK, Chakrabarty R, Mostafa G, Mukherjee PS. Angew. Chem., Int. Ed 2008;47:8455.
24. Stang PJ, Cao DH, Saito S, Arif AM. J. Am. Chem. Soc 1995;117:6273.
25. Kuehl CJ, Huang SD, Stang PJ. J. Am. Chem. Soc 2001;123:9634. [PubMed: 11572685]
26. Lee SJ, Mulfort KL, O'Donnell JL, Zuo X, Goshe AJ, Wesson PJ, Nguyen ST, Hupp JT, Tiede DM. Chem. Commun 2006;44:4581.

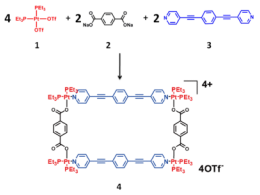

Scheme 1.

Selective self-assembly of a multicomponent rectangle **4** by the combination of *cis*-$Pt(PEt_3)_2(OTf)_2$ **1**, dicarboxylate ligand **2**, and linear dipyridyl donor **3**.

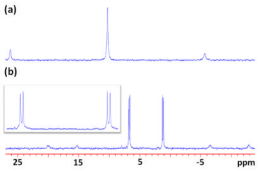

Figure 1.
$^{31}P\{^{1}H\}$ NMR spectra of *cis*-$Pt(PEt_3)_2(OTf)_2$ **1** (a) and the multicomponent supramolecular rectangle **4** (b).

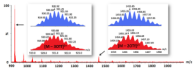

Figure 2.
Full ESI mass spectrum of the solution of the multicomponent supramolecular rectangle **4**.

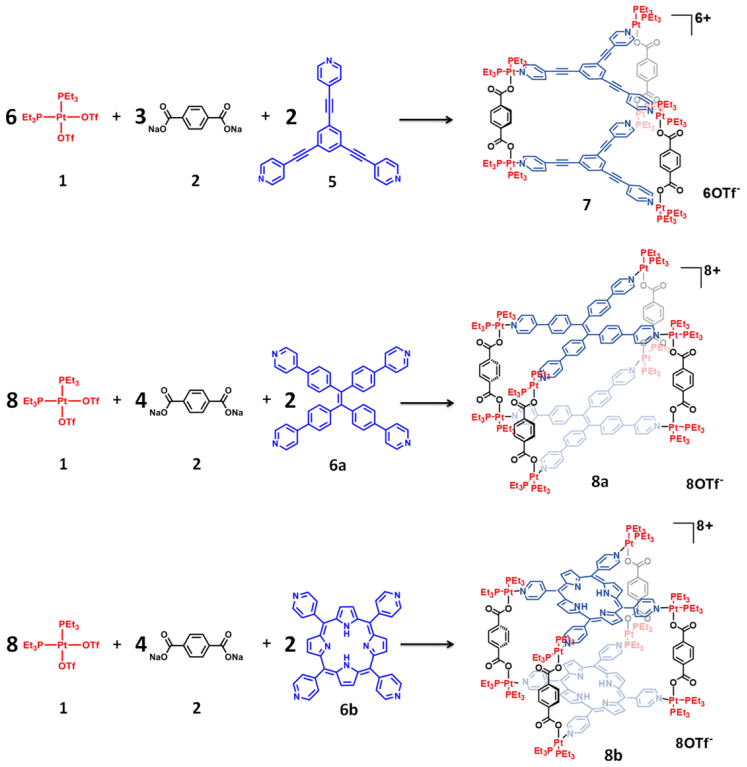

Scheme 2.

Selective self-assembly of multicomponent trigonal (**7**) and tetragonal (**8**) prisms by combination of *cis*-$Pt(PEt_3)_2(OTf)_2$ **1**, dicarboxylate ligand **2**, and tritopic (**5**) and tetratopic (**6**) pyridyl donors.

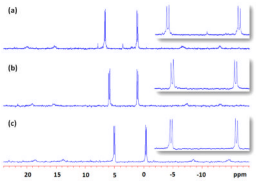

Figure 3.

$^{31}P\{^{1}H\}$ NMR spectra of the trigonal prism **7** (a) and tetragonal prisms **8a** (b) and **8b** (c).

ESI mass spectral data further support the self-assembly of supramolecular prisms **7** and **8**. As shown in Figure 4 and Figure S5,6 (see Supporting Information), intense ESI mass peaks corresponding to consecutive loss of triflate anions from trigonal prism **7**: *m/z* = 2218.76 $[M - 2OTf]^{2+}$ and *m/z* = 1429.59 $[M - 3OTf]^{3+}$ were observed, as were those corresponding to the tetragonal prisms: **8a** at *m/z* = 2037.75 $[M - 3PF_6]^{3+}$ and *m/z* = 1164.50 $[M - 5PF_6]^{6+}$ and **8b** at *m/z* = 2022.71 $[M - 3PF_6]^{3+}$ and *m/z* = 1155.62 $[M - 5PF_6]^{5+}$. All of these peaks are isotopically resolved and agree well with their theoretical distributions.

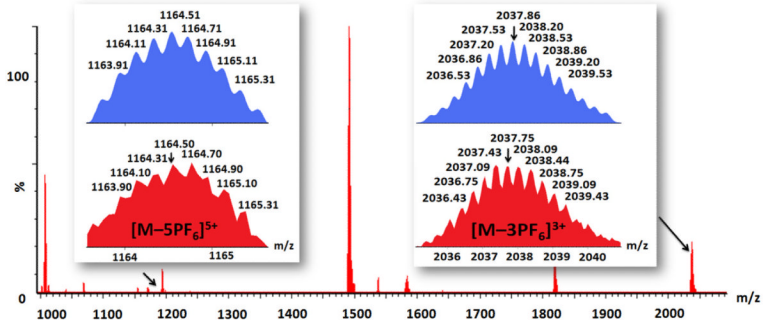

Figure 4.
Full ESI mass spectrum of the tetragonal prism **8a**.

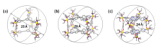

Figure 5.
Computational simulations of trigonal prism **7** (a) and tetragonal prisms **8a** (b) and **8b** (c).

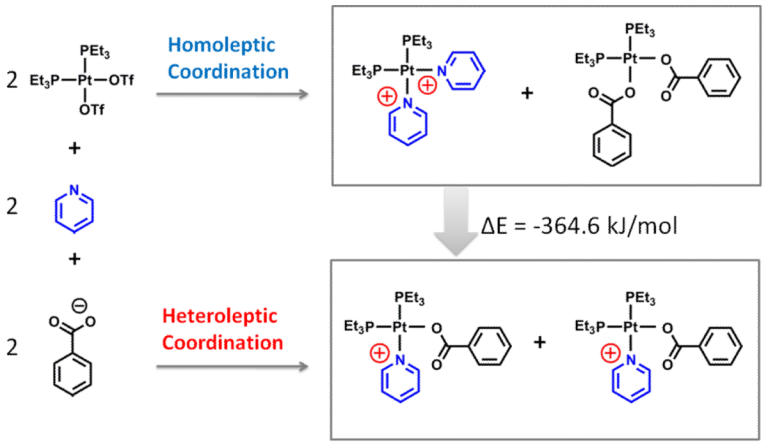

Scheme 3.

Representation of selective self-assembly of *cis*-$Pt(PEt_3)_2(OTf)_2$ with carboxylate and pyridyl moieties due to the lower energy of the heteroleptic System.

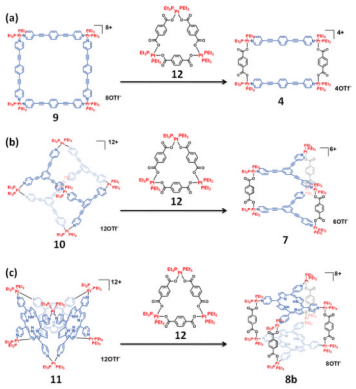

Scheme 4.

Supramolecular transformations of square **9**, truncated tetrahedron **10**, and trigonal prism **11** into rectangle **4**, trigonal prism **7**, and tetragonal prism **8b**, respectively, upon addition of the neutral triangle **12** assembled by *cis*-$Pt(PEt_3)_2(OTf)_2$ **1** and carboxylate ligand **2**.

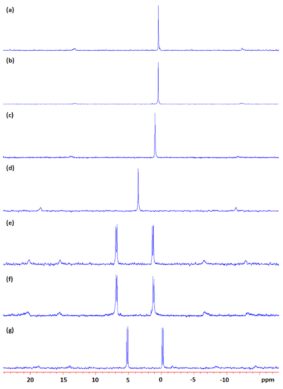

Figure 6.

$^{31}P\{^{1}H\}$ NMR spectra of the homoleptic self-assemblies **9** (a), **10** (b), and **11** (c), and the neutral triangle **12** (d), as well as the multicomponent rectangle **4** (e), trigonal prism **7** (f), and tetragonal prism **8b** (g) obtained via supramolecular transformations.

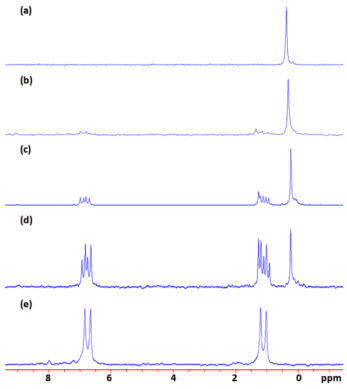

Figure 7.
$^{31}P\{^{1}H\}$ NMR spectra for mixtures of square **9** upon addition of 0% (a), 10% (b), 25% (c), 50% (d), and 100% (e) of neutral triangle **12**.

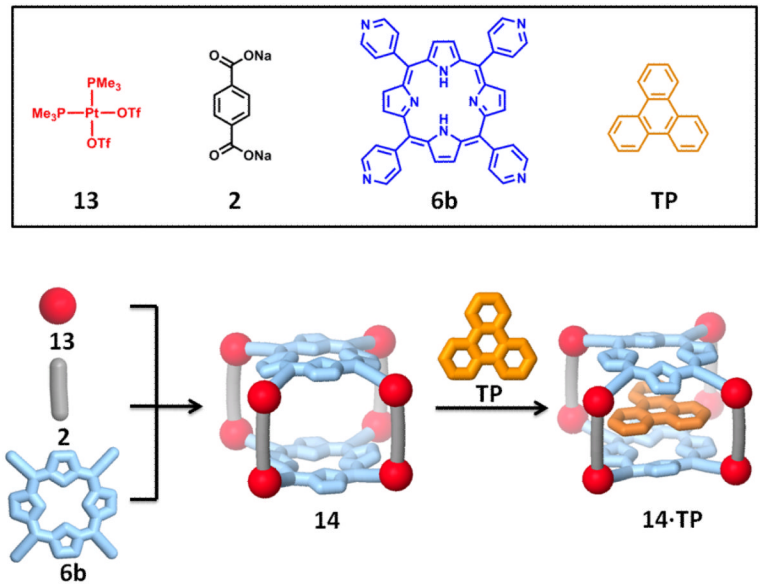

Scheme 5.

Graphical representation of self-assembly of multicomponent porphyrin cage **14** by *cis*-$Pt(PMe_3)_2(OTf)_2$ **13** with carboxylate **2** and pyridyl ligands **6b** and encapsulation of triphenylene **TP**.

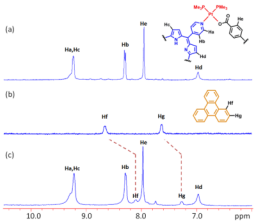

Figure 8.
Partial ^{1}H NMR spectra (300 MHz, acetone-d_6/D_2O = 1:1) of pure **14** (a), **TP** (b), and the host-guest mixture (c).

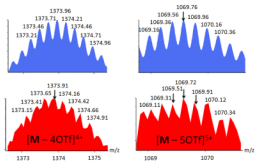

Figure 9.
Calculated (blue, top) and Experimental (red, bottom) ESI mass spectrum of the encapsulated complex **14·TP**.

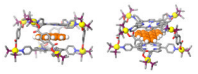

Figure 10.
Varied views of the computational model (MM2*) of the encapsulated complex **14·TP**.